A dipole loudspeaker with a balanced directivity pattern

Tim Mellow[a)]
Nokia UK Ltd., Nokia House, Summit Avenue, Farnborough, Hants GU14 0NG, United Kingdom

Leo Kärkkäinen
Nokia Research Center, Itämerenkatu 11-13, 00180 Helsinki, Finland

(Received 3 March 2010; revised 1 September 2010; accepted 2 September 2010)

Analytical equations describing radiation characteristics of an oscillating ring in a circular finite baffle are derived, including the limiting case of a dipole point source at the center. An oscillating sphere would represent the ideal dipole source, having a constant directivity pattern at all frequencies, but would be inconvenient to realize especially in portable devices. It is found that a planar piston with uniform surface velocity but variable phase arranged to emulate the sphere does not have such a smooth on-axis response as the sphere. Instead a planar piston with the same phase distribution but uniform pressure represents an ideal planar source with a smooth on-axis response and near constant directivity. The surface velocity is plotted and it is then shown that a similar response can be achieved using a finite number of concentric rings based on this velocity distribution. © *2010 Acoustical Society of America.* [DOI: 10.1121/1.3493446]

PACS number(s): 43.38.Hz, 43.20.Bi, 43.20.Rz, 43.38.Ar [TDM] Pages: 2749–2757

I. INTRODUCTION

In recent years, interest in finding analytical solutions to the problems of axisymmetric radiators in an infinite baffle has continued, whether the surface velocity distribution be uniform[1] or non-uniform.[2–4] Cases where the surface velocity is unknown are particularly challenging and have been approached in a number of different ways, which are interesting to compare.[2,4,5] The same kinds of approaches also have to be applied to axisymmetric radiators in free space where the surface pressure distributions are unknown. For example, Aarts *et al.*[4] use a trial function based on Zernike[6,7] polynomials to good effect in order to solve the reverse problem for a resilient radiator in an infinite baffle: By measuring the nearfield axial pressure, the surface velocity distribution can be evaluated.

In the first part of this paper, a derivation is presented for the sound field of a ring source in a circular baffle or, by means of superposition of fields, any number of concentric ring sources. By driving these ring sources with signals of differing amplitudes and phases, a highly-focused or widely-dispersed sound field can be synthesized. The latter has found applications in loudspeakers because producing a spatially omnidirectional source at all frequencies would normally require a very small source size, but producing enough volume velocity from such a source is always not possible.[8] Hence an attractive solution is to use an extended source with annular rings, which can be combined to produce omnidirectional far field pattern. However, traditional approaches[8] assume the need to attenuate the output of the outer rings at high frequencies using lossy delay lines in order to minimize edge diffraction effects, but what is really desired is to have constant radiated power with a uniform cosine directivity pattern. Here this is shown to best achieved by keeping the surface pressure distribution uniform and adjusting the phase, which produces virtually no diffraction effects.

In the next part, the relative velocity amplitudes and phases of the rings are optimized. The ring patterns could be carefully driven electrostatic, piezoelectric or electret speaker designs.[9]

Although transducer arrays are traditionally evaluated in an infinite baffle for computational simplicity, the free space case is often closer to reality and enables a truer picture of the low frequency limit to be ascertained.

In this paper, the Bouwkamp[10]-Streng[11] trial function is used, which is based on the solution to the Helmholtz wave equation in oblate spheroidal coordinates. It is the simplest function and has been found by the authors to converge just as well as any other. Although the power series matching method has been found to be the most efficient for unbaffled radiators,[12,13] the least-mean-squares method, as used here, appears to save processing power for a ring or piston in a finite baffle, because the integrals are all solved analytically, unlike previously where numerical integration had been performed.[14,15]

II. RING AND POINT SOURCE IN A CIRCULAR BAFFLE

A. Boundary conditions

A ring of inner radius a_1 and outer radius a_2 shown in Fig. 1 is mounted in a finite circular baffle of radius b in the xy plane with its center at the origin and oscillates in the z direction with a harmonically time dependent velocity $\tilde{u}_0$, thus radiating sound from both sides into a homogeneous loss-free medium. The dipole source elements shown in Fig. 1 form the disk source. The area of each surface element is given by $\delta S_0 = w_0 \delta w_0 \delta \phi_0$. The pressure field on one side of the xy plane is the symmetrical "negative" of that on the other, so that

[a)]Author to whom correspondence should be addressed. Electronic mail: tim.mellow@nokia.com

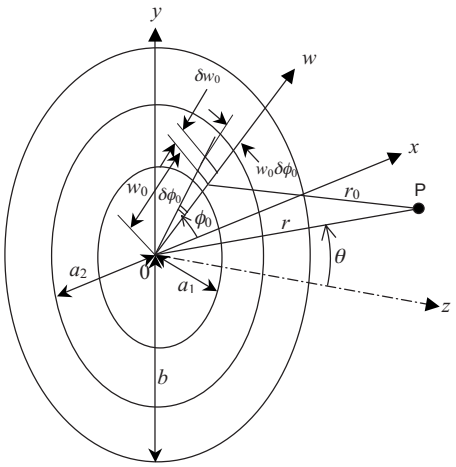

FIG. 1. Geometry of ring in finite baffle. The point of observation P is located at a distance r and angle θ with respect to the origin at the center of the ring.

$$\tilde{p}(w,z) = -\tilde{p}(w,-z). \tag{1}$$

Consequently, there is a Dirichlet boundary condition in the plane of the disk where these equal and opposite fields meet,

$$\tilde{p}(w,0) = 0, \quad b < w \le \infty, \tag{2}$$

which is satisfied automatically. There is also a pressure-gradient boundary condition which is dependent upon the velocity distribution over the disk, ring, or baffle. Streng[11] showed that the front and rear surface pressure distributions $\tilde{p}_+(w_0)$ and $\tilde{p}_-(w_0)$ respectively for any flat axially-symmetric unbaffled source (or sink), based upon Bouwkamp's solution[10] to the free space wave equation in oblate spheroidal coordinates, could be written as

$$\tilde{p}_+(w_0) = -\tilde{p}_-(w_0) = kb\rho c\tilde{u}_0 \frac{a_2^2}{b^2}\sum_{n=0}^{\infty} A_n\left(n+\frac{3}{2}\right)\left(1-\frac{w_0^2}{b^2}\right)^{n+1/2},$$

$$0 \le w_0 \le b, \tag{3}$$

where A_n are the as yet unknown power series coefficient that will be calculated by means of a set of simultaneous equations in matrix form, k is the wave number given by $k = \omega/c = 2\pi/\lambda$, ω is the angular frequency of excitation, ρ is the density of the surrounding medium, c is the speed of sound in that medium, and λ is the wavelength. The tilde denotes a steady-state harmonically-varying quantity, otherwise denoted by the factor $e^{i\omega t}$. In this paper, i represents the positive square root of -1 and is thus equivalent to the imaginary operator j used in circuit theory. Equation (3) is the same as that previously used by the authors[12] with the exception that in its present form it has been multiplied by a_2^2/b^2 in order to facilitate the solution in the limiting case of a point source. This also simplifies subsequent expressions for the radiation impedance and far-field pressure.

B. Formulation of the coupled equation

Although similar derivations are shown in the corresponding sections of previous papers,[12,13] full details are given here for the reader's convenience. The near-field pressure distribution is given by the following dipole boundary integral taking into account the surface pressure on both sides:[16]

$$\tilde{p}(w,z) = \int_0^{2\pi}\int_0^b (\tilde{p}_+(w_0) - \tilde{p}_-(w_0)) \times \frac{\partial}{\partial z_0} g(w,z|w_0,z_0)|_{z_0=0+} w_0 dw_0 d\phi_0, \tag{4}$$

where the Green's function in axisymmetric cylindrical coordinates is given by

$$g(w,z|w_0,z_0) = \frac{-i}{2\pi}\int_0^{\infty} J_0(\mu w)J_0(\mu w_0)\frac{\mu}{\sigma}e^{-i\sigma|z-z_0|}d\mu, \tag{5}$$

where

$$\sigma = \begin{cases} \sqrt{k^2-\mu^2}, & 0 \le \mu \le k, \\ -i\sqrt{\mu^2-k^2}, & \mu > k. \end{cases} \tag{6}$$

In this form Eq. (4) is known as the dipole King integral. Inserting Eqs. (3) and (5) into Eq. (4) and integrating over the surface of the disk and baffle gives

$$\tilde{p}(w,z) = -2ka_2^2\rho c\tilde{u}_0\sum_{n=0}^{\infty} A_n\Gamma\left(n+\frac{5}{2}\right) \times \int_0^{\infty}\left(\frac{2}{\mu b}\right)^{n+1/2} J_0(\mu w)J_{n+3/2}(\mu b)e^{-i\sigma|z|}d\mu, \tag{7}$$

where the following Sonine's integral[17] solution has been used:

$$\int_0^b \left(1-\frac{w_0^2}{b^2}\right)^{n+1/2} J_0(\mu w_0)w_0 dw_0 = \frac{b^2}{2}\Gamma\left(n+\frac{3}{2}\right)\left(\frac{2}{\mu b}\right)^{n+3/2} J_{n+3/2}(\mu b). \tag{8}$$

At the surface of the disk, there is the coupling condition

$$\frac{\partial}{\partial z}\tilde{p}(w,z)|_{z=0+} = -ik\rho c\tilde{u}_0\Phi(w), \tag{9}$$

where $\Phi(w)$ is a dimensionless function of the surface velocity distribution. In this paper different expressions for $\Phi(w)$ will be used when considering a ring or point source in a circular baffle. This leads to the following coupled equation:

$$\sum_{n=0}^{\infty} A_n I_n(w) = -\Phi(w), \tag{10}$$

which is to be solved for the power series coefficients A_n. The integral $I_n(w)$ can be split into two parts,

$$I_n(w) = I_{nR}(w) - iI_{nI}(w), \tag{11}$$

where the real part is given by

$$I_{nR}(w) = a_2^2\Gamma\left(n+\frac{5}{2}\right)\int_0^k \left(\frac{2}{\mu b}\right)^{n+1/2} J_{n+3/2}(\mu b)J_0(\mu w) \times\sqrt{k^2-\mu^2}d\mu, \tag{12}$$

and the imaginary part is given by

$$I_{nI}(w) = a_2^2\Gamma\left(n+\frac{5}{2}\right)\int_k^\infty \left(\frac{2}{\mu b}\right)^{n+1/2} J_{n+3/2}(\mu b) \times J_0(\mu w)\sqrt{\mu^2-k^2}d\mu. \tag{13}$$

The solutions to these integrals can be shown[12,18] to be given by

$$I_{nR}(w) = \sqrt{\pi}\frac{a_2^2}{b^2}\sum_{m=0}^{\infty}\sum_{r=0}^{\infty}\frac{(-1)^{m+r}\Gamma\left(n+\frac{5}{2}\right)\Gamma(m+r+1)}{(m!)^2 r!\Gamma\left(r+n+\frac{5}{2}\right)\Gamma\left(m+r+\frac{5}{2}\right)} \times\left(\frac{kb}{2}\right)^{2(m+r)+3}\left(\frac{w}{b}\right)^{2m}, \tag{14}$$

$$I_{nI}(w) = \sqrt{\pi}\frac{a_2^2}{b^2}\sum_{m=0}^{\infty}\sum_{r=0}^{\infty}\frac{(-1)^{m+r+n}\Gamma\left(n+\frac{5}{2}\right)\Gamma\left(m+r-n-\frac{1}{2}\right)}{(m!)^2 r!\Gamma\left(r-n-\frac{1}{2}\right)\Gamma(m+r-n+1)} \times\left(\frac{kb}{2}\right)^{2(m+r-n)}\left(\frac{w}{b}\right)^{2m}. \tag{15}$$

C. Solution of the power series coefficients for a ring in a circular baffle

In the case of a disk or membrane in free space, the power-series matching method[12,13] gives best results, but for disk or finite ring in a circular baffle, a more efficient method is to employ the following least-mean-squares (LMS) algorithm. From Eq. (10), let an error function be defined by

$$E(A_n) = \int_0^b \left|\sum_{n=0}^{\infty} A_n I_n(w) + \Phi(w)\right|^2 wdw, \tag{16}$$

where

$$\Phi(w) = \begin{cases} 0, & 0 \le w < a_1, \\ 1, & a_1 \le w \le a_2, \\ 0, & a_2 < w \le b. \end{cases} \tag{17}$$

In order to find the values of A_n that minimize the error, the derivative of E is taken with respect to A_n and the result equated to zero,

$$\frac{\partial}{\partial A_n}E(A_n) = 2\int_0^b I_m^*(w)\left(\sum_{n=0}^{\infty} A_n I_n(w) + \Phi(w)\right)wdw = 0, \tag{18}$$

which after truncating the infinite series limit to order N, yields the following set of $N+1$ simultaneous equations

$$\sum_{n=0}^{N} A_n\int_0^b I_m^*(w)I_n(w)wdw = -\int_{a_1}^{a_2} I_m^*(w)wdw, \quad m = 0,1,\cdots,N, \tag{19}$$

where

$$I_m^*(w) = \frac{a_2^2}{b^2}\sum_{p=0}^{P}({}_m\mathbf{S}_p(kb) + i\ {}_m\mathbf{B}_p(kb))\left(\frac{w}{b}\right)^{2p}, \tag{20}$$

$$I_n(w) = \frac{a_2^2}{b^2}\sum_{q=0}^{Q}({}_n\mathbf{S}_q(kb) + i\ {}_n\mathbf{B}_q(kb))\left(\frac{w}{b}\right)^{2q}. \tag{21}$$

The dipole cylindrical wave functions ${}_n\mathbf{B}_m$ and ${}_n\mathbf{S}_m$ are named the Bouwkamp[10] and Streng[18] functions respectively in honor of their pioneering work and are defined by

$${}_n\mathbf{B}_m(kb) = \sqrt{\pi}\sum_{r=0}^{R}\frac{(-1)^{m+r}\Gamma\left(n+\frac{5}{2}\right)\Gamma(m+r+1)}{(m!)^2 r!\Gamma\left(r+n+\frac{5}{2}\right)\Gamma\left(m+r+\frac{5}{2}\right)} \times\left(\frac{kb}{2}\right)^{2(m+r)+3}, \tag{22}$$

$${}_n\mathbf{S}_m(kb) = \sqrt{\pi}\sum_{r=0}^{R}\frac{(-1)^{m+r+n}\Gamma\left(n+\frac{5}{2}\right)\Gamma\left(m+r-n-\frac{1}{2}\right)}{(m!)^2 r!\Gamma\left(r-n-\frac{1}{2}\right)\Gamma(m+r-n+1)} \times\left(\frac{kb}{2}\right)^{2(m+r-n)}. \tag{23}$$

Integrating over w yields the following $N\times N$ matrix equation:

$$\mathbf{M}\cdot\mathbf{a} = \mathbf{b}, \tag{24}$$

where the matrix $\mathbf{M}$ and vectors $\mathbf{a}$ and $\mathbf{b}$ are given by

$$\mathbf{M}(m+1,n+1) = \sum_{p=0}^{P}\sum_{q=0}^{Q}\frac{({}_m\mathbf{B}_p(kb) - j\ {}_m\mathbf{S}_p(kb))}{p+q+1}({}_n\mathbf{B}_q(kb) - j\ {}_n\mathbf{S}_q(kb)), \begin{cases} m = 0,1,\cdots,N, \\ n = 0,1,\cdots,N, \end{cases} \tag{25}$$

$$\mathbf{b}(m+1) = -\sum_{p=0}^{P}\frac{({}_m\mathbf{B}_p(kb) - j\ {}_m\mathbf{S}_p(kb))}{p+1}\left(\left(\frac{a_2}{b}\right)^{2p} - \left(\frac{a_1}{b}\right)^{2p}\left(\frac{a_1}{a_2}\right)^2\right), \quad m = 0,1,\cdots,N, \tag{26}$$

$$\mathbf{a}(n+1) = A_n, \quad n = 0,1,\cdots,N, \tag{27}$$

and the infinite power series limits have been truncated. In the computations, it found to be sufficient to let $N = 10 + 2ka$ and $P = Q = R = 2N$.

D. Solution of the power series coefficients for a point source in a circular baffle

The surface velocity distribution of an infinitesimally narrow ring source of radius a_1 in a circular baffle is given by

$$\Phi(w) = \tfrac{1}{2} a_1 \delta(w - a_1), \tag{28}$$

where δ is the Dirac delta function. Inserting this into Eq. (18) and truncating the infinite series limit to order N, while letting $a_2 = a_1$, yields the following set of $N+1$ simultaneous equations:

$$\sum_{n=0}^{N} A_n \int_0^b I_m(w) I_n(w) w dw = -\frac{a_1}{2} \int_0^b \delta(w - a_1) I_m(w) w dw, \quad m = 0, 1, \cdots, N, \tag{29}$$

where $I_m(w)$ and $I_n(w)$ are given by Eqs. (20) and (21) respectively. Integrating over w and using the property of the Dirac delta function yields the same matrix equations as Eqs. (24)–(27) except that

$$\mathbf{b}(m+1) = -\sum_{p=0}^{P} ({}_m\mathbf{B}_p(kb) - i\ {}_m\mathbf{S}_p(kb)) \left(\frac{a_1}{b}\right)^{2p}. \tag{30}$$

In the limiting case of a point source at the center of a circular baffle, let $a_1 \to 0$ so that

$$\mathbf{b}(m+1) = -({}_m\mathbf{B}_0(kb) + i\ {}_m\mathbf{S}_0(kb)). \tag{31}$$

E. Far-field pressure

The far-field pressure distribution is given by the dipole boundary integral of Eq. (4), but using the far-field Green's function in spherical-cylindrical coordinates:

$$\tilde{p}(r,\theta) = \int_0^{2\pi} \int_0^b (\tilde{p}_+(w_0) - \tilde{p}_-(w_0)) \times \frac{\partial}{\partial z_0} g(r,\theta,\phi|w_0,\phi_0,z_0)\Big|_{\phi=\pi/2}^{z_0=0+} w_0 dw_0 d\phi_0, \tag{32}$$

where the far-field Green's function is given by[16]

$$g(r,\theta,\phi|w_0,\phi_0,z_0) = \frac{1}{4\pi r} e^{-ik(r - w_0 \sin\theta \cos(\phi-\phi_0) - z_0 \cos\theta)}. \tag{33}$$

Due to axial symmetry, there is no ϕ dependency so that any value can be chosen and a value of $\pi/2$ turns out to be the most convenient for solving the angular integral. Inserting Eqs. (3) and (33) into Eq. (32) and integrating over the surface, using Eq. (8) and[17]

$$\frac{1}{2\pi} \int_0^{2\pi} e^{it \sin\phi_0} d\phi_0 = J_0(t) \tag{34}$$

(with $t = kw_0 \sin\theta$, $\mu = k \sin\theta$, and letting $\phi = \pi/2$ so that $\cos(\phi - \phi_0) = \sin\phi_0$ in Eq. (34)), gives

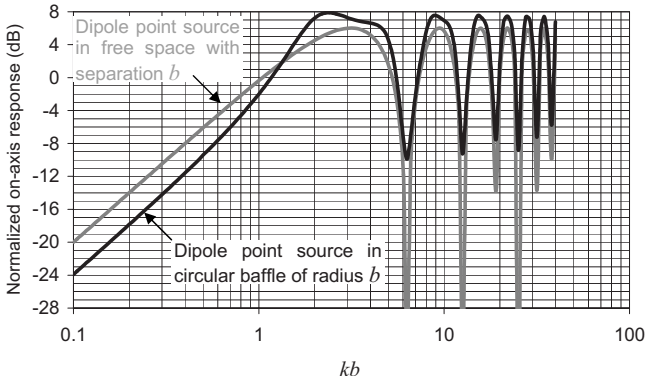

FIG. 2. Normalized far-field on-axis response of a dipole point source in a circular open baffle with constant volume acceleration.

$$\tilde{p}(r,\theta) = ika_2^2 \rho c \tilde{u}_0 \frac{e^{-ikr}}{2r} D(\theta), \tag{35}$$

where the directivity function $D(\theta)$ is given by

$$D(\theta) = kb \cos\theta \sum_{n=0}^{N} A_n \Gamma\left(n + \frac{5}{2}\right) \times \left(\frac{2}{kb \sin\theta}\right)^{n+3/2} J_{n+3/2}(kb \sin\theta). \tag{36}$$

The on-axis pressure is evaluated by setting $\theta = 0$ in Eq. (33) before inserting it in Eq. (32) and integrating over the surface to give

$$D(0) = kb \sum_{n=0}^{N} A_n, \tag{37}$$

so that the on-axis response can be written as

$$\tilde{p}(r,0) = -i\rho_0 f \tilde{U}_0 \frac{e^{-ikr}}{r} kb \sum_{n=0}^{N} A_n, \tag{38}$$

where $\tilde{U}_0 = \pi a_2^2 \tilde{u}_0$ is the total volume velocity in the case of $a_1 = 0$. The on-axis response $20 \log_{10}(D(0))$ of a point source in a circular baffle of radius b is plotted in Fig. 2. In the same figure there is also plotted the response in free space of two point sources of opposite phase on the same axis with a separation of b, which is given by $20 \log_{10}|e^{ikb/2} - e^{-ikb/2}|$ or $20 \log_{10}|2i \sin kb/2|$. Using the superposition of fields, the on-axis response of a monopole point source in a closed circular baffle is obtained by combining the dipole point source in an open circular baffle with a monopole point source in free space to obtain

$$D(0) = \frac{1}{2}\left(1 + kb \sum_{n=0}^{N} A_n\right). \tag{39}$$

The on-axis response $20 \log_{10}(D(0))$ is plotted in Fig. 3. In the same figure there is also plotted the response in free space of two point sources of opposite phase, as before, but with a monopole source half way between them, which is given by $20 \log_{10}|(1 + e^{ikb/2} - e^{-ikb/2})/2|$ or $20 \log_{10}|(1 + 2i \sin kb)/2|$.

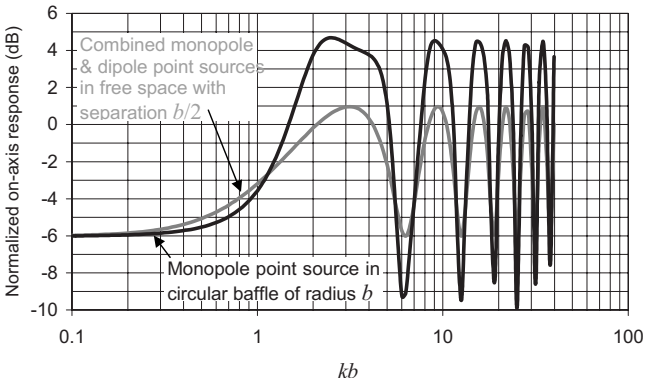

FIG. 3. Normalized far-field on-axis response of a monopole point source in a circular closed baffle with constant volume acceleration.

F. Radiation impedance of a ring in a circular baffle

The total radiation force is found by integrating the pressure from Eq. (3) over the surface of the ring on both sides to give

$$\tilde{F} = -\int_0^{2\pi}\int_{a_1}^{a_2} (\tilde{p}_+(w_0) - \tilde{p}_-(w_0))w_0 dw_0 d\phi. \tag{40}$$

The specific radiation impedance Z_s is then given by $Z_s = \tilde{F}/\tilde{U}_0 = R_s + jX_s$, where $\tilde{U}_0 = \pi(a_2^2 - a_1^2)\tilde{u}_0$ is the total volume velocity. The specific radiation resistance R_s per side is given by

$$R_s = kb\rho c \frac{a_2^2}{a_2^2 - a_1^2}\Re\left(\sum_{n=0}^{N} A_n \left\{\left(1 - \frac{a_1^2}{b^2}\right)^{n+3/2} - \left(1 - \frac{a_2^2}{b^2}\right)^{n+3/2}\right\}\right), \tag{41}$$

and the specific radiation reactance X_s per side is given by

$$X_s = kb\rho c \frac{a_2^2}{a_2^2 - a_1^2}\Im\left(\sum_{n=0}^{N} A_n \left\{\left(1 - \frac{a_1^2}{b^2}\right)^{n+3/2} - \left(1 - \frac{a_2^2}{b^2}\right)^{n+3/2}\right\}\right). \tag{42}$$

III. VIRTUAL OSCILLATING SPHERE

An ideal dipole sound source is the oscillating sphere which has a perfectly smooth monotonic far-field pressure response and a constant dipole directivity pattern. Three ways to emulate this kind of sound source using a flat circular radiator are described in this section. In Section III A this is done using a driving velocity distribution of uniform magnitude. In Section III B, the uniform velocity distribution is exchanged for a uniform pressure distribution. In each case a continuously variable delay is applied to the driving velocity or pressure, where the delay path length is $b - \sqrt{b^2 - w_0^2}$ as can be seen from Fig. 4. In Section III C a velocity source is used, but the velocity magnitude and phase distribution is discretized using separate rings, where the velocity at the midpoint along the radius of each ring is matched to that of the corresponding point on pressure source of Section III B.

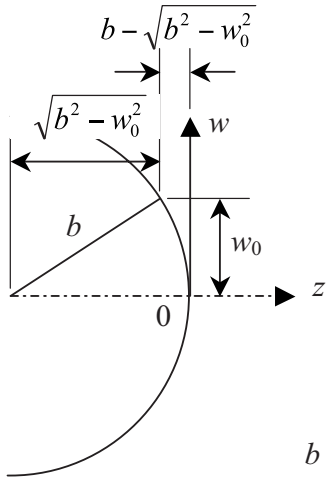

FIG. 4. Sketch showing geometry of hemispherical delay path length.

A. Virtual oscillating sphere using a planar source with uniform surface velocity but variable delay

A surface velocity distribution which has an increasing delay toward the rim in order to simulate an oscillating sphere of radius b is given by

$$\Phi(w) = e^{ik(b - \sqrt{b^2 - w^2})} = e^{ikb(1 - \sqrt{1 - w^2/b^2})}, \tag{43}$$

where the delay path length at the rim is the radius b of the sphere. Inserting this into Eq. (18) and truncating the infinite series limit to order N yields the following set of $N+1$ simultaneous equations:

$$\sum_{n=0}^{N} A_n \int_0^b I_m^*(w) I_n(w) w dw = -\int_0^b e^{ikb(1 - \sqrt{1 - w^2/b^2})} I_m^*(w) w dw, \quad m = 0, 1, \cdots, N, \tag{44}$$

where $I_m(w)$ and $I_n(w)$ are given by Eqs. (20) and (21) respectively. Integrating over w yields the same matrix equations as Eqs. (24)–(27) except that

$$\mathbf{b}(m+1) = -\sum_{p=0}^{P} ({}_m\mathbf{S}_p(kb) - i\,{}_m\mathbf{B}_p(kb))\frac{2}{b^{2p+2}} \times \int_0^b e^{ikb(1 - \sqrt{1 - w^2/b^2})} w^{2p+1} dw. \tag{45}$$

The on-axis response and directivity patterns plotted from Eqs. (37) and (36) are shown in Fig. 5 and Fig. 6 respectively. For comparison, the on-axis response of an oscillating sphere is also included using[16] $D(0) = 2ikb/(2 - k^2b^2 + 2ikb)$.

B. Virtual oscillating sphere using a planar source with uniform surface pressure but variable delay

If the loudspeaker is a pressure transducer, as are typically electrostatic types, the surface pressure can be approximated by a uniform driving pressure $\tilde{p}_0$ so that applying the delay of Eq. (43) gives

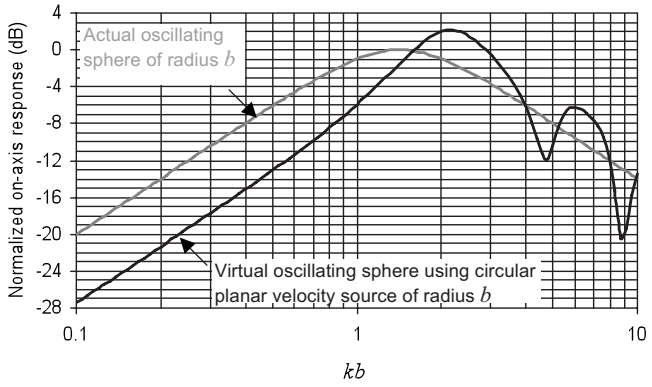

FIG. 5. Normalized far-field on-axis response of virtual oscillating sphere using a planar source with uniform surface velocity magnitude but variable delay. Plot is of $20\log_{10}(|D(0)|)$ where $D(0)$ is given by Eq. (37).

$$\tilde{p}_+(w_0) = -\tilde{p}_-(w_0) = \frac{\tilde{p}_0}{2} e^{ikb(1-\sqrt{1-w_0^2/b^2})}, \quad 0 \le w_0 \le b. \tag{46}$$

Inserting Eqs. (46) and (33) into Eq. (32) and integrating over the surface, using Eq. (34) yields

$$\tilde{p}(r,\theta) = -ib\tilde{p}_0 \frac{e^{-ikr}}{4r} D(\theta), \tag{47}$$

where after substituting $w_0 = bs$ the directivity factor is given by

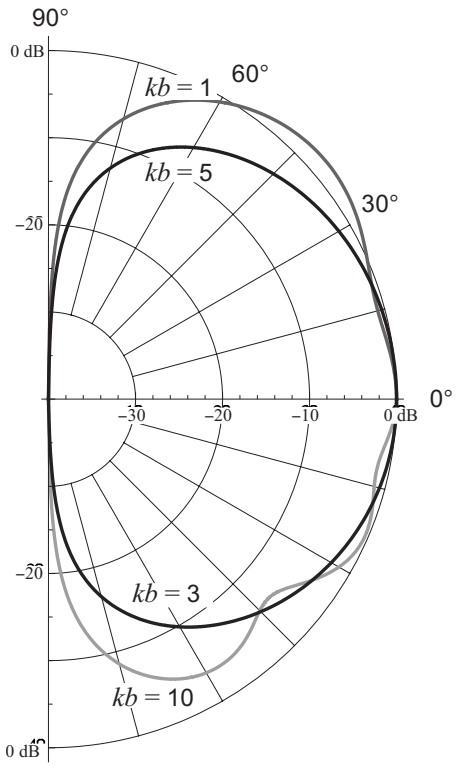

FIG. 6. Normalized far-field directivity pattern of virtual oscillating sphere using a planar source with uniform surface velocity magnitude but variable delay. Plot is of $20\log_{10}(|D(\theta)|/|D(0)|)$ where $D(\theta)$ is given by Eq. (36) and $D(0)$ is given by Eq. (37).

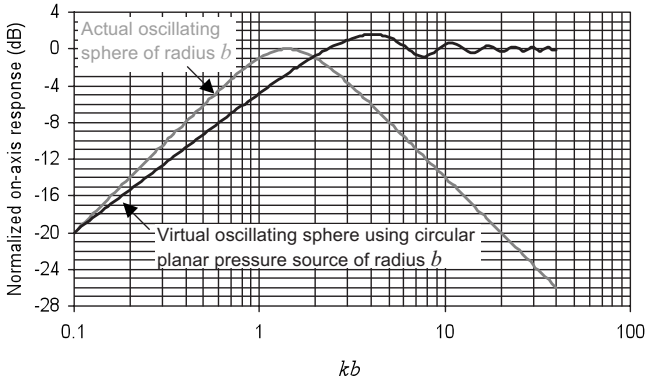

FIG. 7. Normalized far-field on-axis response of virtual oscillating sphere using a planar source with uniform surface pressure magnitude but variable delay. The same frequency response shape can also be obtained from a planar source in an infinite baffle with uniform surface velocity magnitude but variable delay, where the velocity is constant at all frequencies. Plot is of $20\log_{10}(|D(0)|)$ where $D(0)$ is given by Eq. (49).

$$D(\theta) = 2kb\cos\theta \int_0^1 e^{ikb(1-\sqrt{1-s^2})} J_0(kbs\sin\theta) s\,ds. \tag{48}$$

For the on-axis response, a closed-form solution is given by

$$D(0) = \frac{2}{kb}(1 - e^{ikb} + ikb). \tag{49}$$

The on-axis response and directivity patterns plotted from Eqs. (49) and (48) are shown in Fig. 7 and Fig. 8 respectively. The nearfield pressure is given by Eq. (4) using the Green's function of Eq. (5) and surface pressure distribution

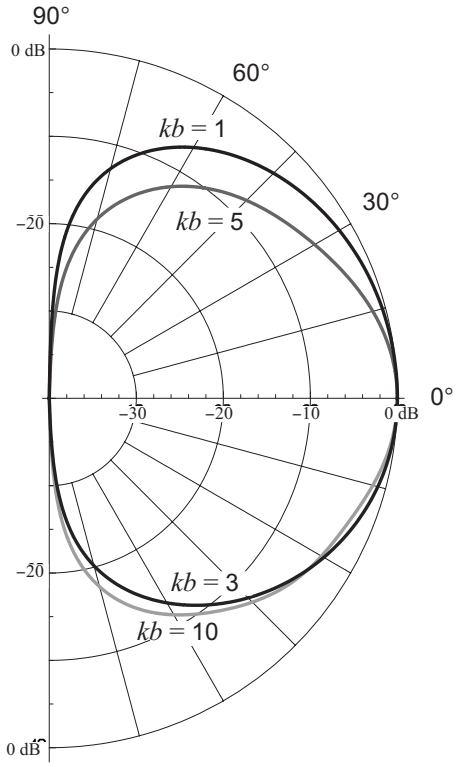

FIG. 8. Normalized far-field directivity pattern of virtual oscillating sphere using a planar source with uniform surface pressure magnitude but variable delay. Plot is of $20\log_{10}(|D(\theta)|/|D(0)|)$ where $D(\theta)$ is given by Eq. (48) and $D(0)$ is given by Eq. (49).

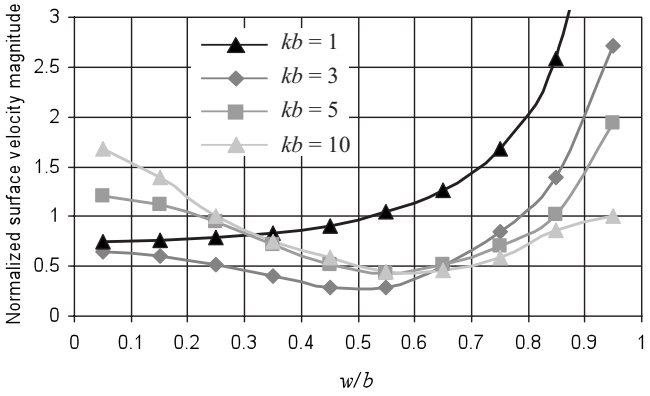

FIG. 9. Normalized surface velocity magnitude of the planar source with uniform surface pressure magnitude but variable delay. Plot is of $2\rho c|\tilde{u}_0(w)|/|\tilde{p}_0|$, where $\tilde{u}_0(w)$ is given by Eq. (51).

of Eq. (46). The surface velocity of the delayed pressure source is calculated by inserting the delay from Eq. (46) into Eq. (81) from Ref. 19 for the near pressure field resilient disk in free space. Letting $r_1=\sqrt{z^2+w_0^2}$, $r_a=\sqrt{z^2+b^2}$, and $\cos\beta = z/r_1$ gives

$$\tilde{p}(w,z) = \frac{ik\tilde{p}_0}{\sqrt{\pi}}\sum_{n=0}^{\infty}(-1)^n(4n+3)\frac{\Gamma\left(n+\frac{3}{2}\right)}{\Gamma(p+1)} \times \frac{j_{2n+1}(kw)}{w}\int_0^b h_{2n+1}^{(2)}(k\sqrt{z^2+w_0^2}) \times P_{2n+1}\left(\frac{z}{\sqrt{z^2+w_0^2}}\right)w_0 dw_0. \quad (50)$$

From this the surface velocity is given by

$$\tilde{u}_0(w) = \frac{1}{-ik\rho c}\frac{\partial}{\partial z}\tilde{p}(w,z)|_{z\to 0}, \quad 0 \le w \le b. \quad (51)$$

The normalized magnitude and phase of the surface velocity is plotted in Fig. 9 and Fig. 10 respectively.

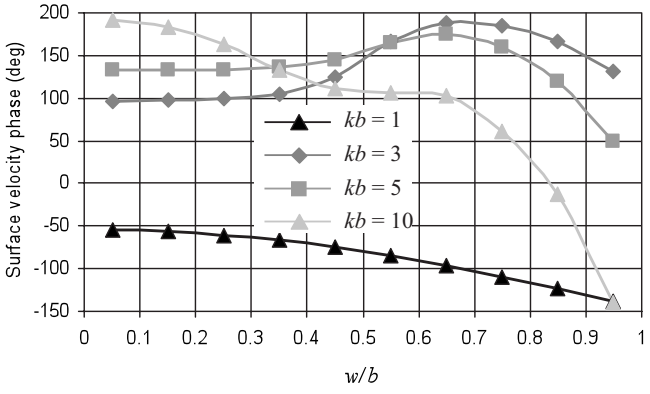

FIG. 10. Normalized surface velocity phase of the planar source with uniform surface pressure magnitude but variable delay. Plot is of $\angle\tilde{u}_0(w)$, where $\tilde{u}_0(w)$ is given by Eq. (51).

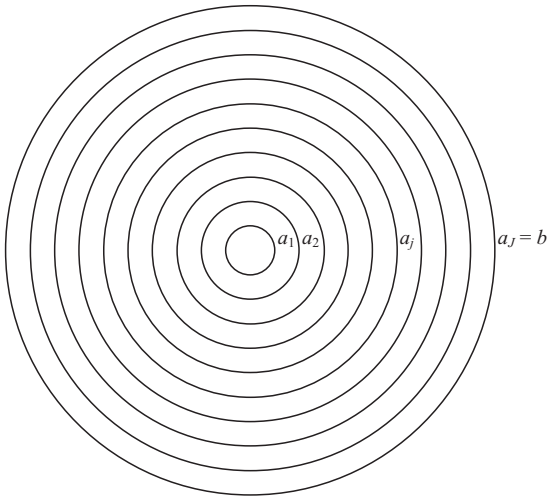

FIG. 11. Geometry of planar concentric ring sources. Plot is of $\pi\arg(\tilde{u}_0(w))/180$ where $\tilde{u}_0(w)$ is given by Eq. (51).

C. Virtual oscillating sphere using a planar array of concentric ring radiators

As an application for the solutions it is shown here how an array of concentric radiators can be optimized to provide an even sound field. First assume that the radiator in question is a plane with a center element and a number of surrounding rings as shown in Fig. 11. The standard way to solve the directivity problem in plane radiators would be to make the radiating surface long in vertical and narrow in horizontal direction. However, this will not help if the device with the loudspeaker is portable, and one cannot predict before hand how the user is going to hold it. Thus, a circular solution is better—in particular as an upwards radiating circular speaker element is not directional at all in the horizontal direction.

The far field representation of the sound is the summation over j of each element from Eqs. (35) and (36),

$$\tilde{p}(r,\theta) = -ika_j^2\rho c\frac{e^{-ikr}}{2r}\sum_{j=1}^{J}\tilde{u}(a_j)D_j(\theta), \quad (52)$$

where the directivity functions $D(\theta)$ are given by even functions

$$D_j(\theta) = kb\cos\theta\sum_{n=0}^{N}A_{nj}\Gamma\left(n+\frac{5}{2}\right) \times\left(\frac{2}{kb\sin\theta}\right)^{n+3/2}J_{n+3/2}(kb\sin\theta), \quad (53)$$

and the complex velocity for each ring $\tilde{u}_0(a_j)$ is obtained from Eq. (51). The on-axis response then becomes

$$D_j(0) = kb\sum_{n=0}^{N}A_{nj}. \quad (54)$$

IV. DISCUSSION

The dipole point source in a circular baffle is the limiting case of a disk in a circular baffle[12] where the radius of the disk is infinitesimally small. Unlike a circular disk of

finite radius, the peaks in the response of the baffled dipole point source (see Fig. 2) show no sign of diminishing with increasing frequency. In the case of a circular disk[12] where the baffle radius is eight times that of the disk, the shape of the first maximum is virtually identical to that of the baffled dipole point source. However, the remaining maxima are progressively diminished due to the fact that the disk becomes more directional at high frequencies.

It is interesting to compare the on-axis response of the baffled dipole point source with that of a dipole point source in free space (see Fig. 2), which is a classic comb filter. Although their minima are perfectly aligned, the maxima of the baffled point source are shifted slightly and a couple of dBs higher due to reflections at the rim of the baffle giving rise to radial resonance modes. The low frequency radiation from the baffled point source is weaker than that of the dipole in free space due to a stronger anti-phase rear-wave emerging at the rim which has spread out hemispherically from the center. This is in contrast to the dipole in free space where the anti-phase radiation from the furthest point source spreads out spherically.

Similar differences as those just described can be seen between the two monopole responses shown in Fig. 3. The overall shift of 6 dB in the output between low frequencies and high frequencies can be explained by the fact that when the wavelength is much greater than the radius of the baffle, the monopole point source effectively radiates into whole space, but when the wavelength is short, the source behaves more or less as though the baffle is infinite and thus radiates mainly into half space.

Because a rigid oscillating sphere is an axial velocity source, as opposed to a resilient one which would be a pressure source, one might expect a planar velocity source with a uniform velocity magnitude but the phase delay path length of that shown in Fig. 4 to provide a good approximation. However, although the directivity pattern of Fig. 6 reasonably good, the on-axis response of Fig. 5 is rather irregular at high frequencies. Not surprisingly, it behaves like an oscillating disk in free space at low frequencies, which has a weaker output than an oscillating sphere due to the shorter path length between the rear and front radiating surfaces. Better results are obtained using a pressure source which gives the smooth on-axis response of Fig. 7 and an almost constant directivity pattern that is free of ripples or side lobes, as shown in Fig. 8, which is perhaps slightly surprising because, unlike the oscillating sphere, the surface velocity magnitude shown in Fig. 9 increases toward the rim. This kind of result should be achievable using an electrostatic or electret transducer for high quality reproduction of the electrical signal where the stator electrodes are divided into concentric rings as shown in Fig. 11. An electrostatic or electret loudspeaker is virtually a pure pressure source except that the rim of the membrane is normally clamped, whereas the idealized model used here is freely suspended which produces a singularity at the rim. If a velocity transducer is used, such as an array of electrodynamic loudspeakers, then best results are obtained when velocity distribution is arranged to be the same as that of a pressure transducer. The directivity response of nine concentric rings with a central disk is

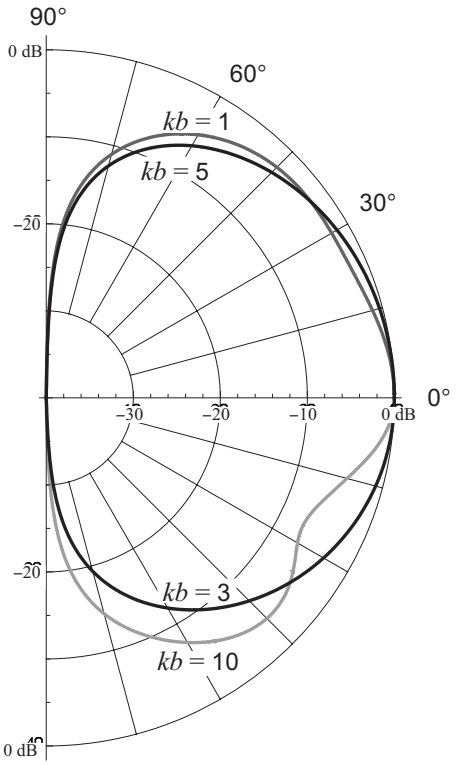

FIG. 12. Normalized far-field directivity pattern with optimized velocities for ten planar rings. Plot is of 20 $\log_{10}(|\Sigma_{j=1}^{10} D_j(\theta)|/|\Sigma_{j=1}^{10} D_j(0)|)$ where $D_j(\theta)$ is given by Eq. (53) and $D_j(0)$ is given by Eq. (54).

shown in Fig. 12. Discretization aside, this should be considered as an approximation to the directivity pattern of the pressure source shown Fig. 8. Because the concentric rings are velocity driven, they have different mutual impedances to those of an array of pressure driven rings. If only one ring is excited in a pressure driven array, it is unaffected by the remaining rings, which are acoustically transparent, whereas in a velocity driven array, the remaining rings are opaque. To illustrate this, the point source in a circular baffle, for which the on-axis response is shown in Fig. 2, may be considered as the central element of the array. Clearly a smoother response is obtained when the baffle is transparent and the point source is located in free space. It is worth mentioning that the on-axis response of Fig. 7 is also obtained from a planar source in an infinite baffle with a uniform velocity magnitude but the phase delay path length of that shown in Fig. 4, where the driving velocity is constant at all frequencies.

V. CONCLUSION

A relatively straightforward analytical solution for the pressure field of annular dipole rings within a finite baffle has been provided. In practice, this is important in future portable devices, where one cannot easily deploy multiple speaker configurations, nor close the back side to a large back cavity. However, large displays will give bigger, although thin, areas to work with which are suitable for dipole electrostatic or electret speakers.[9,20]

The challenge has been how to control optimally the directivity of a large planar source. Here the analytical solu-

tion has been used to specify an axially symmetric segmentation of the planar radiator, with each ring having its own frequency dependent velocity magnitude and phase, which gives a good radiation pattern across a wide range of frequencies as seen in Fig. 12.

The radiation impedances of the rings in a finite baffle have also been provided in order to complete the system model. Although this paper describes the blueprint for a balanced, almost ideal, planar radiating speaker, the realization of a manufacturable design has still many challenges to overcome.

[1]T. D. Mast and F. Yu, "Simplified expansions for radiation from a baffled circular piston," J. Acoust. Soc. Am. **118**, 3457–3464 (2005).
[2]H. Suzuki and J. Tichy, "Sound radiation from an elastically supported circular plate," J. Acoust. Soc. Am. **65**, 106–111 (1979).
[3]J. F. Kelly and R. J. McGough, "An annular superposition integral for axisymmetric radiators," J. Acoust. Soc. Am. **121**, 759–765 (2006).
[4]R. M. Aarts and A. J. Janssen, "Sound radiation quantities arising from a resilient circular radiator," J. Acoust. Soc. Am. **126**, 1776–1787 (2009).
[5]T. J. Mellow and L. M. Kärkkäinen, "Comparison of spheroidal and eigenfunction-expansion trial functions for a membrane in an infinite baffle," J. Acoust. Soc. Am. **123**, 2598–2602 (2008).
[6]F. Zernike, "Beugungstheorie des Schneidensverfahrens und seiner verbesserten Form, der Phasenkontrastmethode (Diffraction theory of the knife-edge test and its improved form, the phase-contrast method)," Physica (Amsterdam) **1**, 689–704 (1934).
[7]M. Born and E. Wolf, *Principles of Optics*, 7th ed. (Cambridge University Press, Cambridge, England, 1999), pp. 523–525 and 905–910.
[8]P. J. Walker, "New developments in electrostatic loudspeakers," J. Audio Eng. Soc. **28**, 795–799 (1980).
[9]T. J. Mellow and L. M. Kärkkäinen, "On the forces in single-ended and push-pull electret transducers," J. Acoust. Soc. Am. **124**, 1497–1504 (2008).
[10]C. J. Bouwkamp, "Theoretical and numerical treatment of diffraction through a circular aperture," IEEE Trans. Antennas Propag. **AP18-2**, 152–176 (1970).
[11]J. H. Streng, "Calculation of the surface pressure on a vibrating circular stretched membrane in free space," J. Acoust. Soc. Am. **82**, 679–686 (1987).
[12]T. J. Mellow and L. M. Kärkkäinen, "On the sound field of an oscillating disk in an open and closed circular baffle," J. Acoust. Soc. Am. **118**, 1311–1325 (2005).
[13]T. J. Mellow and L. M. Kärkkäinen, "On the sound field of a membrane in free space and an infinite baffle," J. Acoust. Soc. Am. **120**, 2460–2477 (2006).
[14]J. H. Streng, "Sound radiation from a circular stretched membrane in free space," J. Audio Eng. Soc. **37**, 107–118 (1989).
[15]T. J. Mellow, "On the mutual radiation characteristics of two rigid discs in open or closed finite circular baffles," Joint Baltic-Nordic Acoustics Meeting 2004, Mariehamn, Åland (8–10 June 2004), available online at http://www.acoustics.hut.fi/asf/bnam04/webprosari/onlineproc.html (Last viewed September 1, 2010).
[16]P. M. Morse and K. U. Ingard, *Theoretical Acoustics* (McGraw-Hill, New York, 1968), Eq. (7.1.17), pp. 321, 315–317, 389–390.
[17]I. S. Gradshteyn and I. M. Ryzhik, *Table of Integrals, Series, and Products*, 6th ed., A. Jeffrey, ed. (Academic, New York, 2000), Eq. (6.567.1), Eq. (8.411.1), pp. 671 and 902.
[18]J. H. Streng, "Calculation of integrals which occur in the analysis of circular stretched membrane sound radiation," J. Acoust. Soc. Am. **83**, 1183–1185 (1988).
[19]T. J. Mellow, "On the sound field of a resilient disk in free space," J. Acoust. Soc. Am. **123**, 1880–1891 (2008).
[20]M. R. Bai, C.-J. Wang, D.-M. Chiang, and S.-R. Lin, "Experimental modeling and design optimization of push-pull electret loudspeakers," J. Acoust. Soc. Am. **127**, 2274–2281 (2010).